Superclusters of galaxies

II. Distribution and correlation functions

M. Kalinkov, I. Valtchanov, and I. Kuneva

Institute of Astronomy, Bulgarian Academy of Sciences, 72 Tsarigradsko Chausse blvd, 1784 Sofia, Bulgaria
(e-mail: markal@phys.acad.bg, ivan@astro.acad.bg) (Fax: (359 2) 755-019)

Abstract. Surface and space distributions of samples of superclusters of galaxies in the catalog of superclusters of Kalinkov & Kuneva (1995) – Paper I, is investigated. Galactic latitude selection and declination selection functions are found. The wavelet transform technique is used for the surface distribution. It is established that the structures of superclusters with highest density are in fact noise fluctuations. Gaussian smoothing and filtering is also used with the same result. Space distribution is presented and distance selection functions are estimated. We have found that the voids among superclusters of galaxies follow Poisson distributions in the 2D as well as in the 3D case. Two-point space correlation functions do not differ significantly from zero, but the crosscorrelation functions supercluster-cluster are well defined. Attempts are made to verify the conclusions. The main result is that superclusters located in galactic polar caps for the distance interval $100 \leq R\,h^{-1}$ Mpc ≤ 627 are distributed randomly. There are no structures consisting of superclusters of galaxies.

Key words: (cosmology:) large-scale structure of Universe – galaxies: clusters: general – methods: statistical

1. Introduction

The space distribution of galaxies reveals the existence of a large diversity of structures – pairs, multiplets and groups, also loose and rich, compact and open clusters, as well as filaments, chains, sheets, walls, likewise voids (at least among galaxies and clusters). From the observational point of view, a current paradigm is that the superclusters of galaxies are the highest order of clustering, although some assumptions of huge structures have been made – Batuski & Burns (1985a,b), Tully (1987), Chamaraux et al. (1990), despite that there is no definitive evidence for such structures (e.g. Postman et al. 1989).

It is not clear now what is the distribution of the superclusters. The distance and galactic selection functions are also unknown. The reason is the small number of superclusters in the existing lists and catalogs (Rood 1976, Murray et al. 1978, Karachentsev & Shcherbanovski 1978, Thuan 1980, Kalinkov et al. 1983, Bahcall & Soneira 1984, Batuski & Burns 1985a, West 1989, Postman et al. 1992, Zucca et al. 1993, Einasto et al. 1994), insufficient to draw any conclusion. Only the last catalog of Einasto et al. (1997) contains 220 superclusters.

The study of the surface and space distribution of the superclusters is the main motivation for this paper, which is the second in a series. The first one (Kalinkov & Kuneva 1995, hereafter KK) contains the largest catalog of superclusters found among A- and ACO-clusters of galaxies (Abell 1958, Abell et al. 1989) with superclusters defined for local density enhancements f = 10, 20, 40, 100, 200 and 400.

The second motivation is connected with the existence of a transition scale to an isotropic and homogeneous Universe. The power spectrum $P(k) \propto k^n$, where k is the wavenumber, gives an idea for the distribution of galaxies and clusters of galaxies as a function of scale. The spectral index is $-2 < n < -1$ for a few tens of Mpc (e.g. Peacock 1991, Peacock & Nicholson 1991). When the scale increases, the spectrum flattens (Peacock & West 1992, Vogeley et al. 1992, Vogeley 1995, Fisher et al. 1993). The transition from negative to positive spectral index is somewhere between 100 and 400 h^{-1} Mpc. Einasto & Gramann (1993) give for the correlation transition scale $130 \pm 10\,h^{-1}$ Mpc, while the spectral transition scale is $175 \pm 15\,h^{-1}$ Mpc. This is in accordance with the detection of fluctuations of the cosmic microwave background radiation on scales about 1000 h^{-1} Mpc, consistent with the Harrison-Zeldovich spectrum of perturbations with $n = 1$ (Smooth et al. 1992). Is there any transition scale for superclusters?

Sect. 2 concerns the redshift estimates used for the A-clusters without any measured redshift. The surface distribution of the superclusters is studied in Sect. 3, where galactic latitude selection and declination selection functions are found, while the space distribution is examined in Sect. 4, where distance- de-

pendent densities, connected with distance selection functions are given.

In Sect. 5, existence of voids among superclusters of galaxies is investigated. Estimates of the 2-point space correlation function of superclusters are presented in Sect. 6. The reliability of the conclusions is studied in Sect. 7.

The third paper in the series will examine the kinematics and dynamics of superclusters – elongation, shape, radii and crossing times, mass and statistics of their characteristics.

All cosmologically-dependent values are given for $H_0 = 100\,\mathrm{km\,s^{-1}Mpc^{-1}}$ and $q_0 = 0.5$. Luminosity distance is used. Note that some authors use proper motion or parallax distance.

2. Redshift estimates for clusters of galaxies

The distances to most of the clusters used in KK are not measured but estimated. The necessary formulae for multiple regression redshift estimates are given by Kalinkov et al. (1994). Some considerations for uncertainty of the distance estimates are presented by Kalinkov & Kuneva (1995).

Here we adduce some figures to afford an opportunity for comparison between measured and estimated redshift.

Our attempts to find common acceptable multiple regressions for "northern" clusters from Abell (1958) catalog, A1 – A2712, as well as for "southern" (Abell et al. 1989), A2713 – A4076, failed. Moreover, different cluster characteristics require various regressions.

Northern clusters. Fig. 1 is the Hubble diagram for the tenth-rank galaxies (n = 961 clusters) and for the first-rank galaxies. Diagrams $(\hat{z}, z)$ and $(\hat{z} - z, z)$ where $\hat{z}$ is the redshift estimate are given in Fig. 2. Apparently $\hat{z}$ to z correspondence is linear up to $z \approx 0.2$.

Southern clusters. Other multiple regressions lead to diagrams $(\hat{z}, z)$ and $(\hat{z} - z, r)$ for $n = 186$ clusters, presented in Fig. 3.

Finally, the multiple regression redshift estimates are consistent for northern clusters, but the estimates for southern clusters should be treated with caution.

3. Surface distribution of superclusters

The first surface presentation of the groups of clusters of galaxies found by Rood (1976) is given by him (Rood 1979). A more refined surface distribution of superclusters, defined at various density enhancements from a complete sample of Abell clusters is examined by Bahcall & Soneira (1984). Up to now there are no definitive conclusions for the 2D distribution of superclusters of galaxies.

We have studied some samples from the KK catalog of superclusters in the distance range $100 \leq R\,\mathrm{Mpc} \leq 627$. The sample, including superclusters having multiplicity $\nu = 2$ from the entire catalog, are denoted in Table 1, where sample sizes are given. Designations 2 and 3 indicate multiplicity $\nu \geq 2$ and $\nu \geq 3$ respectively; N and S stand for north and south polar cap, and 30 and 40 are the low limits of the galactic latitude (degrees). Thus 3N30 means the samples consisting of all su-

Table 1. Sample sizes of superclusters in distance interval $100 \leq R\,\mathrm{Mpc} \leq 627$

Sample	Density contrast					
	10	20	40	100	200	400
2N30	292	319	295	237	179	132
2S30	350	377	334	239	183	134
2N30z	124	131	130	104	84	58
2S30z	105	103	90	71	57	40
2N40	230	242	229	186	143	105
2S40	302	320	284	204	155	113
2N40z	101	104	104	84	71	47
2S40z	87	85	73	60	48	33
3N30	126	94	68	38	20	11
3S30	131	95	65	31	16	10
3N30z	64	49	38	21	13	5
3S30z	49	30	17	8	2	1
3N40	102	75	53	26	13	6
3S40	113	83	53	25	11	6
3N40z	52	40	29	13	9	3
3S40z	41	29	14	7	2	1

perclusters having $\nu \geq 3$ and $b \geq +30°$, disregarding whether the distance to a member cluster is defined from measured or estimated redshift. In the other case, the 3N30z sample consists of those superclusters which have at least one cluster member at the lowest density enhancement with measured redshift. *All superclusters with member clusters having estimated redshift only are disregarded.* When needed the density enhancement is added as an extension – 3N30.100.

We regard samples 3N30 and 3S30 as the most representative ones, especially to search for a dependence on galactic latitude. The problem of the galactic latitude selection function for superclusters is untouched for the small sample sizes of previous catalogs.

Dividing the galactic caps $|b| \geq 30°$ into belts (bins) defined by parallels and denoting with n_0 the number of superclusters in any belt and with n_r – the corresponding number of randomly distributed points, we have

$$K = \frac{n_0}{n_r} = \mathrm{dex}\left[\alpha\left(1 - \mathrm{cosec}|b|\right) + \beta\right]. \tag{1}$$

We have experimented with 3, 4, 5 and 6 equal area belts as well as in (non-equal area) belts with equal numbers of superclusters. The results are more stable when equal area belts are used, and there is no need to generate random objects in this case. Thus, the linear regression is

$$\log K = \alpha\left(1 - \mathrm{cosec}|b|\right) + \beta, \tag{2}$$

where α is the parameter representing the galactic absorption. In fact, α, β and their errors vary strongly with the number of bins. We have computed many regressions and chosen those which have the smallest standard deviation of the regression and the highest correlation coefficient r between "observed" and fitted values of $\log K$.
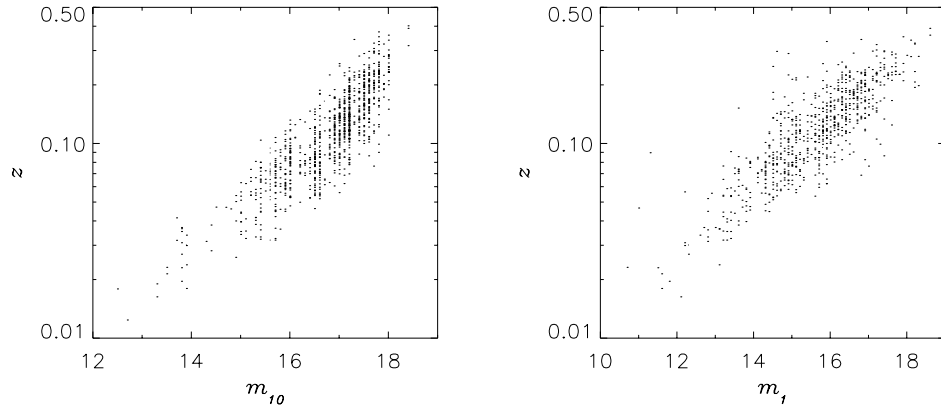
Fig. 1. Hubble diagram for northern (Abell) clusters of galaxies: left panel for tenth, right panel for first-ranked galaxy
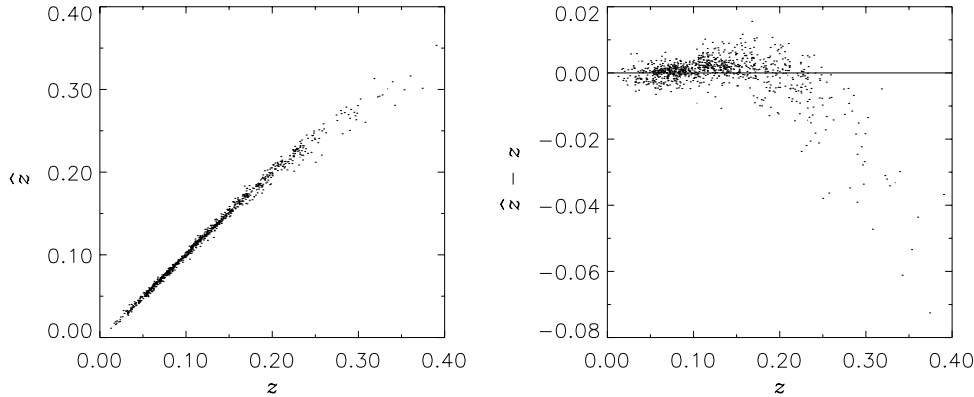
Fig. 2. Relations between estimated $\hat{z}$ and measured z redshift for northern clusters: diagrams $(\hat{z}, z)$ and $(\hat{z} - z, z)$
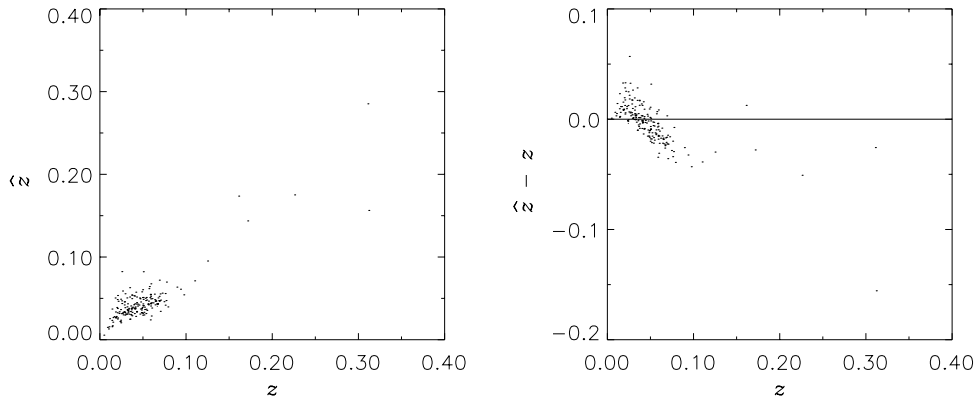
Fig. 3. Southern (ACO) clusters of galaxies: diagrams $(\hat{z}, z)$ and $(\hat{z} - z, z)$

The results for samples 3N30, 3N30z, 3S30 and 3S30z are presented in Table 2, which contains the density enhancement f, fitting parameters α and β together with their standard deviations, the correlation coefficient r, st. dev. of the regression s and the number of bins.

For sample 3N30.10 of superclusters, we have α = 0.45 ± 0.04. According to Bahcall & Soneira (1983), this coefficient for northern clusters is 0.3. Postman et al. (1992) worked with α = 0.32 for A-clusters with $m_{10} \leq 16.5$. Romani & Maoz (1992) found a larger coefficient, namely 0.53 for the Abell statistical sample.

We have estimated α for northern clusters (n = 1055 with richness group $\mathscr{R} \geq 1$) from the Abell statistical sample and

found α = 0.32 ± 0.14 (just the Bahcall & Soneira value!), r = 0.79 and s = 0.08. But for **all** clusters having $b \geq 30°$, n = 1719, we get α = 0.26 ± 0.05, r = 0.97, s = 0.02.

For sample 3S30.10, the coefficient is α = 0.72 ± 0.02. Bahcall et al. (1988) and Batuski et al. (1989) defined α = 0.2 for the southern clusters of galaxies. But keeping in mind that our supercluster catalog is based on Abell and ACO clusters of galaxies, we have estimated α for all clusters having $b \leq -30°$ (n = 1893). The result is α = 0.52 ± 0.02 with r = 1.0 and s = 0.01.

The galactic latitude selection is stronger for superclusters than for clusters of galaxies. It seems that galactic absorption influences southern superclusters more than northern ones.

Table 2. Galactic latitude selections

Sample	f	α	$\Delta\alpha$	β	$\Delta\beta$	r	s	Bins
3N30	10	0.45	0.04	0.16	0.02	0.99	0.02	3
	20	0.49	0.04	0.17	0.02	0.99	0.02	4
3N30z	10	0.43	0.07	0.15	0.03	0.97	0.04	4
	20	0.53	0.11	0.18	0.05	0.98	0.05	3
3S30	10	0.72	0.02	0.24	0.01	1.00	0.01	3
	20	0.56	0.07	0.19	0.03	0.99	0.03	3
3S30z	10	0.70	0.09	0.23	0.04	0.99	0.04	3
	20	1.53	0.31	0.44	0.14	0.98	0.14	3

Therefore the galactic latitude selection function for northern and southern superclusters is

$$P(b) = 10^{\alpha(1-\operatorname{cosec}|b|)} \tag{3}$$

with $\alpha = 0.47$ and 0.64 for north and south, respectively (averaged for $f = 10$ and 20). We give the results for samples 3N30z and 3S30z only for comparison. They are not so reliable (in this case!), as the sample size is smaller. Nevertheless, they show that samples with and without measured z do not differ significantly (with the exception of 3S30z.20 where the sample size is only 30).

Another selection effect is recognized by Olowin et al. (1987) – dependence on declination. According to Bahcall et al. (1988) and Batuski et al. (1989), the declination selection is very clearly pronounced for ACO-clusters. For $-75° < \delta < -20°$, they found $P(\delta) = 10^{0.6(\cos|\delta|-1)}$, while for the northern hemisphere of the Abell sample $P(\delta) = 0.675 + 0.0112\delta$ for $-27° < \delta < 24°$ and $P(\delta) = 1$ for $24° < \delta < 90°$. The total Abell sample shows no significant declination dependence.

Postman et al. (1992) did not find any declination selection for the A-clusters with $m_{10} \leq 16.5$. A declination bias for fainter clusters from the ACO catalog is more evident.

In our case, to study the declination effect, we have the difficulty of having some A- and ACO-clusters in one and the same supercluster.

We have applied the idea of Scaramella et al. (1991b) and found

$$K' = \frac{n_0}{n_r} = 10^{\alpha'(1-\sec\zeta)+\beta'}, \tag{4}$$

where $\zeta = |\varphi - \delta|$ with φ – the latitude of the observatory where plates are taken.

Our results show no declination selection for sample 3N30.10, where members of superclusters are presumably A-clusters. When 5 superclusters containing ACO-clusters are excluded $K' \approx 1$ again. However there is an excess of 25% of observed over random superclusters for $0° < \zeta < 10°$.

For sample 3S30.10, no declination selection is found when all superclusters are used. But for 59 superclusters with only ACO-clusters, we got $\alpha' = 1.99 \pm 0.11$, $\beta' = 0.31 \pm 0.2$, $r = 1.00$ and $s = 0.03$ for 3 bins. There are 60 superclusters with only A-clusters as members. The corresponding $K' \approx 1$.

We conclude that superclusters with A-clusters only are not subject to declination selection. Contrarily, for the ACO-superclusters there is strong declination selection. This confirms the result of Batuski et al. (1989) for ACO-clusters.

The search for declination selection is made with mock catalogs generated with our galactic latitude selections $P(b)$, using the rejection method (Press et al. 1992).

The apparent distribution of superclusters (circles) for samples 3N30.10 and 3S30.10 is presented in Fig. 4. The centers are the galactic poles and the outside circles are at $|b| = 30°$. Galactic latitude, right ascension and declination are also denoted. This is the equal area azimuthal Lambert projection. In such a projection Lambert coordinates could be defined:

$$
\begin{aligned}
x &= 2\sin l \sin\left[\left(90° - |b|\right)/2\right]\\
y &= 2\cos l \sin\left[\left(90° - |b|\right)/2\right]
\end{aligned}
\tag{5}
$$

with polar distance $r = 2\sin\left[\left(90° - |b|\right)/2\right]$. We use this projection to study the apparent distribution of superclusters in more detail.

We generated a grid in Lambert coordinates so that the grid is inscribed to the parallel $|b| = 30°$. Thus $-\sqrt{2}/2 \leq x,\ y \leq \sqrt{2}/2$. The orientation of the axes with respect to galactic coordinates is given in Figs. 5–6. The circle indicate $|b| = 60°$, while $0°$ and $90°$ refer to galactic longitude.

Now it is simple to apply the wavelet transform introduced by Morlet (Gaupllaud et al. 1984). The wavelet analysis is described in detail for investigation of clustering and subclustering of galaxies elsewhere, e.g. Slezak et al. (1990, 1993, 1994), Escalera & Mazure (1992), Escalera et al. (1992), Grebenev et al. (1995), Escalera & MacGillivray (1995, 1996), Biviano et al. (1996). That is why we present no formulae here. It is enough to say that we use a Mexican hat on a grid of 64×64 with a complete set of scales a, $2a$, $4a$, $6a$, ... $16a$. An elementary cell of the grid is $1.266° \times 1.266° = 1.6\,\square°$. Thus we have computed 9 images of the wavelet coefficients for each sample investigated. In our case, when galactic latitude selection is established, it is impossible to use any periodic boundary conditions. We hope the edge effects do not substantially alter our results.

The wavelet image at $16a = 20.2°$ for sample 3N30.10 is presented in Fig. 5. Dotted lines show negative wavelet coefficients. It is evident that the highest isolines of the wavelet coefficients are not centered on the NGP. There are two factors influencing isoline positions – a deficiency of clusters of galaxies in the second quadrant (hence deficiency of superclusters) and an excess of clusters (and excess of superclusters) in the fourth quadrant. However more discussion is needed.

Abell (1958) remarked that there is a significant shortage of clusters of galaxies around $l \approx 330°$ up to latitude $60°$, indicating the presence of considerable galactic obscuration. Shane & Wirtanen (1954) obtained low galaxy counts (cf. Shane & Wirtanen 1967) in this region. Concerning the fourth quadrant, Bahcall & Soneira (1982) found a void in the distribution of nearby (distant groups $\mathscr{D} \leq 4$), rich ($\mathscr{R} \geq 1$) Abell clusters. The void extends to $(\sim 300) \times (\gtrsim 60) \times (\sim 150)\,\mathrm{Mpc}^3$.
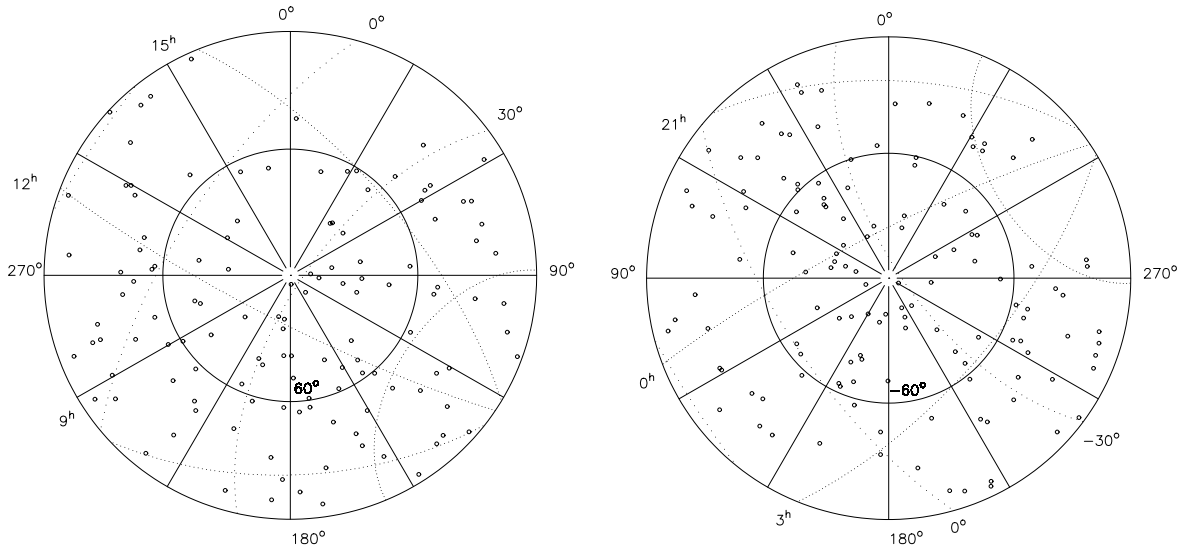
Fig. 4. Distribution of superclusters on equal area projection. The outside circle is for $|b| = 30°$. Galactic longitudes, RA and DEC are denoted: left panel for 3N30.10, right panel for 3S30.10
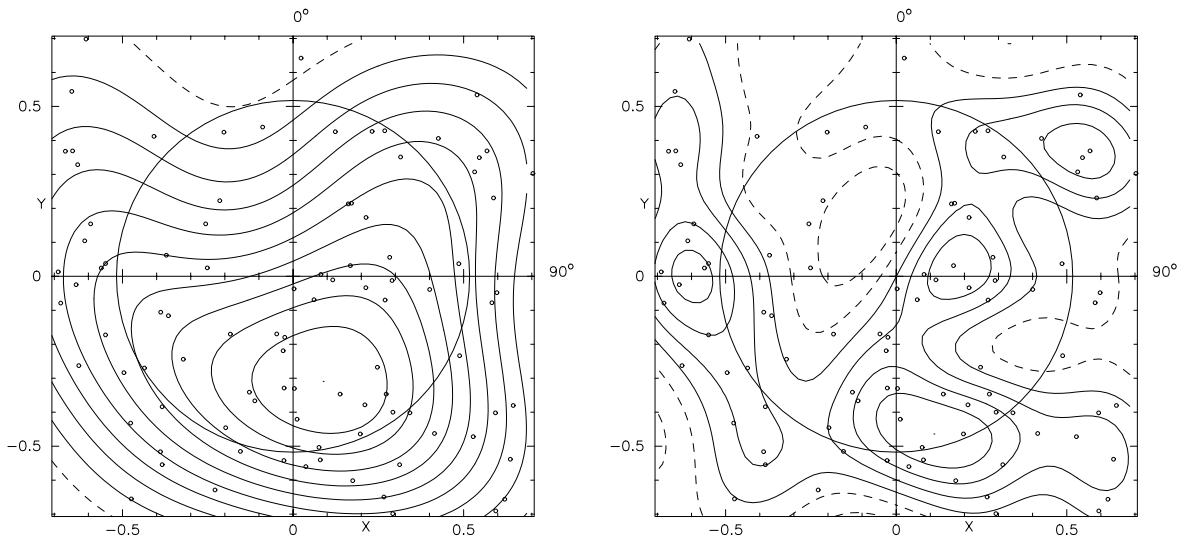
Fig. 5. Wavelet images. Dotted lines show negative wavelet coefficients: left panel for 3N30.10 at $16a = 20.2°$, right panel at $8a = 10.1°$

In this region, a huge concentration of distant Abell clusters is found, which coincides with a similar one of Zwicky clusters (Kalinkov 1977). According to the map of Holmberg (1974), his Fig. 3, for deviations from a standard galactic absorption law with $\alpha = 0.25$, there is an exceptionally low absorption. In the light of the study of Nichol & Connoly (1996), based on the HI radio map of Stark et al. (1992), it "is extremely difficult to separate extinction-induced clustering from real large-scale structure".

The wavelet image for 3N30.10 at $8a = 10.1°$ is given in Fig. 5. Fig. 6 contains images for 3S30.10 at $16a = 20.2°$ and $8a = 10.1°$, respectively. The highest apparent density of the south superclusters is more or less close to the SGP.
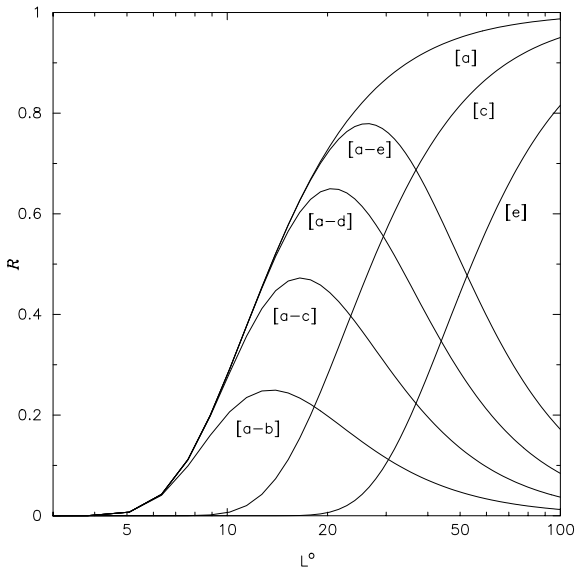
The presence of an apparent superstructuring in Figs. 5–6 requires a discussion of the question whether they are significant. That is why we have to test the significance of maxima of the wavelet coefficients. Two methods were proposed – by Slezak et al. (1990) and by Escalera & Mazure (1992). We use a method closely resembling that of Escalera & Mazure (1992). We generate 3000 simulated "random" supercluster catalogs with the corresponding galactic latitude selection functions, while longitudes are randomly distributed. (We did not find any significant difference using randomly distributed longitudes or randomly drawing out longitudes from the "real" catalog – bootstrap method). Of course, the number of superclusters in mock catalogs is equal to the number of real superclusters. We computed wavelet coefficients for each simulation and counted the number of cases N_{est} when max $c_{sim} >$ max c_{sample}. Thus the probability P that the highest wavelet coefficients in the real fields are fluctuations is

$$P = N_{est}/3000. \qquad (6)$$
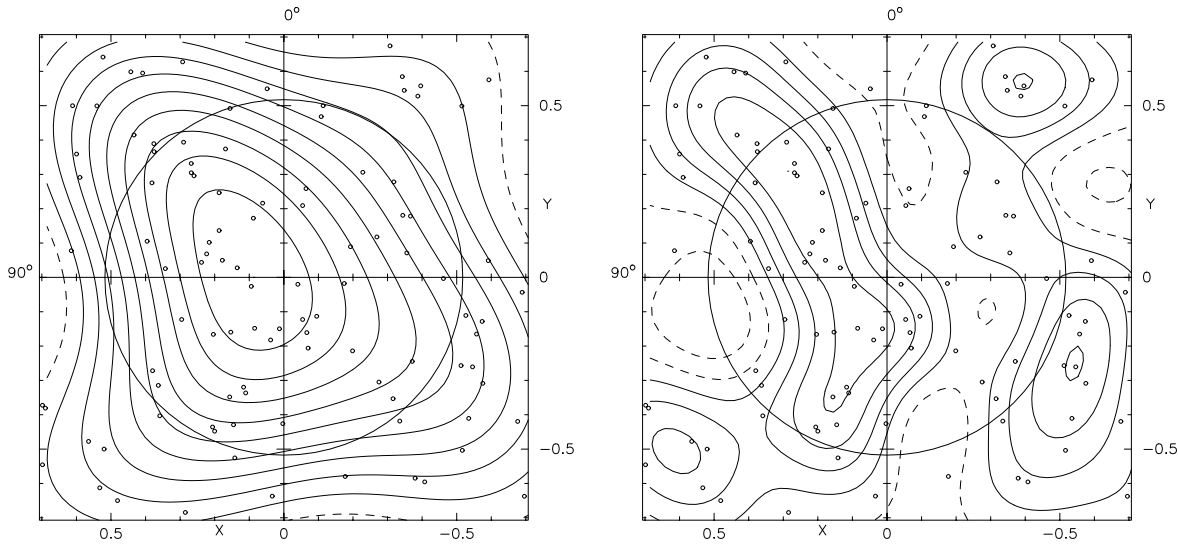
Fig. 6. Wavelet images for sample 3S30.10: left panel at $16a = 20.2°$, right panel at $8a = 10.1°$

Fig. 7. Responses of smoothing and unnormalized filtering functions

Table 3. Probability P that superstructures in Figs. 5–6 are fluctuations

a		Probability P	
Cells	Deg	3N30.10	3S30.10
1	1.27	0.97	0.44
2	2.53	0.83	0.71
4	5.06	0.99	0.81
6	7.60	0.97	0.98
8	10.1	0.95	0.95
10	12.7	0.80	0.85
12	15.2	0.68	0.79
14	17.7	0.57	0.51
16	20.2	0.52	0.19

The difference between the procedure of Escalera & Mazure (1992) and ours is that we examine only the highest coefficient in each simulation.

Results for samples 3N30.10 and 3S30.10 are given in Table 3. The probabilities are in striking disagreement with those obtained by Escalera & Mazure (1992) – they have found for a substructure (in A754) $P < 1/3000(!)$. Table 3 shows that the configurations responding to the highest density peaks are not physical groupings, since they often appear in mock catalogs. This is not a serious argument against any grouping in the examined fields of superclusters. We were not able to investigate all single peaks, and therefore some of them could be a real ones, which do not appear in the simulated catalogs.

Another way to present the apparent distribution of super-clusters of galaxies is to apply simple Gaussian smoothing. We sketch very briefly the technique, described by Kalinkov (1973), Kalinkov et al. (1976, 1987) and applied for searching of sub- and superstructures of galaxies and clusters of galaxies (Kalinkov 1974, 1976, 1977; Kalinkov et al. 1978, 1987).

Let us circumscribe a square again in Lambert coordinates, around the parallel $|b| = 30°$. We construct a grid 114×114 with cells $1°27 \times 1°27$, roughly equal to the cells in the previous grid 64×64. Using the technique (Kalinkov et al. 1987) to avoid edge effects, we smooth supercluster fields inside the parallel $|b| = 30°$.

We use Gaussian smoothing functions denoted by [a], [b], [c], [d], [e] and corresponding filters [a-b], [b-c] . . . [a-c],. . . [a-e]. These functions are part of a complete set whose responses are given by $R_i(L) = \exp\left(-2^i a/L^2\right)$, where $a = \pi^2/8$, while $L = 1/f$ is the characteristic scale length, and $i = 6$ for [a],. . . , $i = 10$ for [e]. This means that the principal cell of the smoothing function contains $0.5\,\sigma$ for [a], $0.5/\sqrt{2}\sigma$ for [b],. . . , 0.125σ for [e], where σ is the standard deviation of the normal distribution $\mathcal{N}(0, 1)$. Fig. 7 presents responses R of smoothing functions

Table 4. Maximum passing $L^\circ{}_{max}$ of the filters

Filter	$L^\circ{}_{max}$
[a-b]	13.6
[b-c]	19.2
[c-d]	27.8
[d-e]	38.4
[a-c]	16.6
[b-d]	23.5
[c-e]	33.3
[a-d]	20.8
[b-e]	29.4
[a-e]	26.3

Table 5. Probability that substructures are fluctuations

Smoothed function	Half-beam width, $\square^\circ$	Probability P	
		3N30.10	3S30.10
[b]	57	1.00	0.65
[c]	114	1.00	0.70
[d]	227	0.94	0.60
[e]	454	0.74	0.38

We have to conclude that at least the highest density peaks among beautiful substructures are real fluctuations. Some of the substructures may be real configurations but their number, if any, is not large.

4. Space distribution

Examples of variation of the supercluster space density D scl Mpc^{-3} with distance R for $|b| \geq 40^\circ$ are presented in Figs. 10–11, together with Poisson errors and linear fits. The linear regression coefficients, corresponding correlation coefficients and st. dev. of regressions are given in Table 6. Generally the regression is

$$\log D = a + b\,R. \tag{7}$$

Merged samples for both galactic caps are denoted with (N+S).

The coefficient a defines the supercluster space density D_0 at redshift $z = 0$. Denoting $D_0 = 10^{-a}$ whence $D/D_0 = $ dex $(-b\,R)$, which is connected with the distance selection function and could be used to generate mock catalogs of superclusters.

Thus $D_0 = 1.2^{+0.6}_{-0.3} \cdot 10^{-6}$ scl Mpc^{-3} for 3N40.10, $D_0 = 1.2^{+0.5}_{-0.4} \cdot 10^{-5}$ scl Mpc^{-3} for 3S40.10, and the mean density (N+S) is $D_0 = 4.06 \cdot 10^{-6}$ scl Mpc^{-3}.

Correspondingly for $f = 20$, we have $D_0 = 1.3 \cdot 10^{-6}$, $8.1 \cdot 10^{-6}$ and $3.53 \cdot 10^{-6}$ scl Mpc^{-3} for N, S and (N+S).

For $f = 40$, we have mean density $D_0 = 1.9 \cdot 10^{-6}$ and for $f = 100 - D_0 = 8.9 \cdot 10^{-7}$ scl Mpc^{-3}.

Samples 3(N+S)40 (Fig. 10) demonstrate the decrease of D_0 when density contrast increases. The slope b, however does not depend on density contrast. A test with sample 3(N+S)40z.10 definitely shows that if we exclude superclusters with members whose redshift is estimated, then the distance selection will be stronger. Samples 3N40 and 3S40 (Fig. 11) allows us to establish the difference between north and south caps. Obviously the distance selection for the south cap is stronger and the space density D_0 is unrealistically high. Since the number of superclusters in the south cap are presumably found among ACO-clusters of galaxies, one has to conclude that the superclusters found among A-clusters form a more representative sample. The mean coefficient $<b> = -0.00094$ for samples 3N40.10-40, while $<b> = -0.0031$ for S samples. The conclusion is supported by samples 3N40.10 and 3S40.10.

It is curious to look at the space density variation of superclusters with multiplicity $\nu \geq 2$. Keeping in mind the superclus-
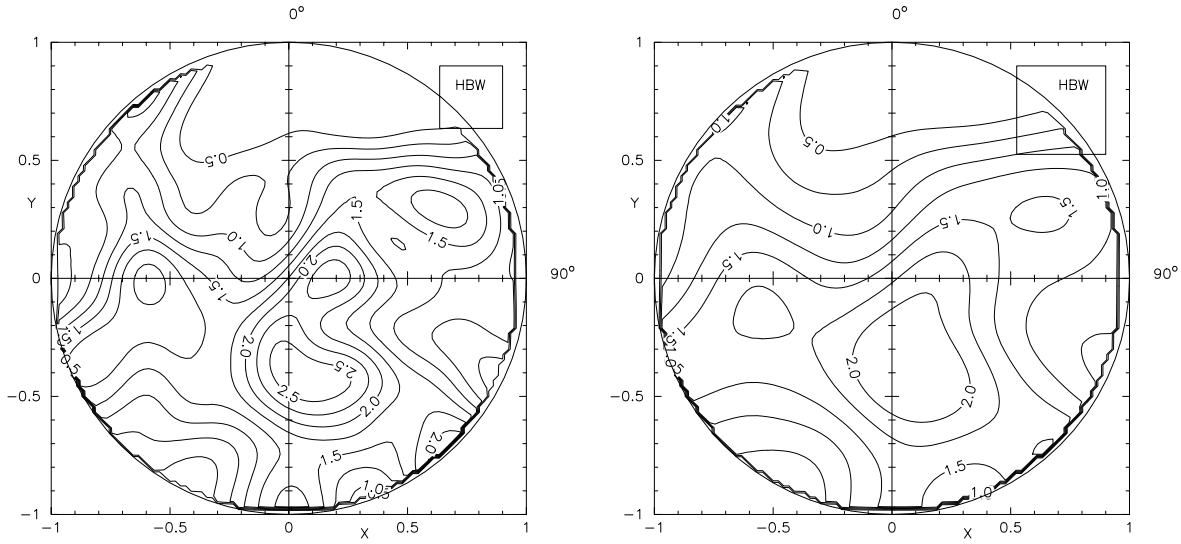
[a], [c], [d] and of filters [a-b], [a-c], [a-d], [a-e]. The filters are not normalized, but their normalization offers no difficulty. Note that the Nyquist frequency is $1/2 \cdot 1.27^\circ$, so the characteristic scale length is defined for $L \geq 2.6^\circ$.

Table 4 contains the maximum passing of the filters.

Smoothed and filtered maps are given in Figs. 8–9. The isopleths are in scl/100 $\square^\circ$. The squares represent HBW of the corresponding smoothing functions.

All figures definitely show that the boundary effects are very small and extend to a few degrees only above $|b| = 30^\circ$. In fact, the method of smoothing and filtering of discrete fields as described by Kalinkov et al. (1987) is applicable to a broad spectrum of problems.

It is interesting to compare wavelet with smoothed maps.

Sample 3N30.10. Fig. 5 (right panel) resembles Fig. 8 (left panel), but Fig. 5 (left panel) is more smoothed than Fig. 8 (right panel).

The same conclusion can be drawn from the other samples.

The wavelet coefficient maps and smoothed (and filtered) maps allow to present structures at almost one and the same way. But as one could see in Figs. 8–9, the smoothing and filtering afford an opportunity to work on one and the same grid with an exceptionally large variety of responses, which might be constructed in advance. This means that smoothing and filtering enables us to search structures at any characteristic scale.

We have smoothed all the samples with sufficient size from Table 1. There are no significant distinctions between corresponding samples for $\nu \geq 2$ and $\nu \geq 3$ for $f = 10$, but samples at $f = 400$ differ from samples at $f = 10$.

There is a considerable substructuring in all the maps. It is quite natural to ask whether the highest peaks are real or if they are fluctuations. This problem may be solved similarly to the way in which the highest wavelet coefficients are tested. We simulate 3000 catalogs of superclusters of galaxies following all selections in the real catalog and count how many times the maximum density in the smoothed simulated fields exceeds the corresponding maximum density in the smoothed real field. It should be mentioned that only the highest density in each field is counted.

The results for two samples are given in Table 5.

Fig. 8. Smoothed sample 3N30.10. Half-beam widths of smoothing functions are denoted: left panel with [d], right panel with [e]
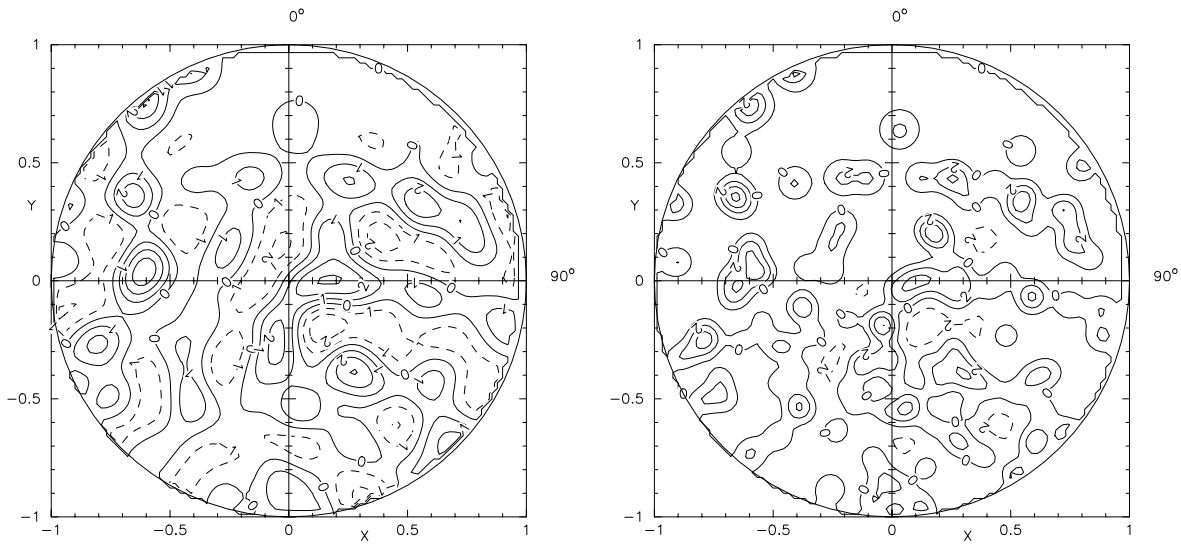
Fig. 9. Sample 3N30.10, processed with normalized filters. Dotted lines present negative densities: left panel with [c-d], right panel with [a–e]
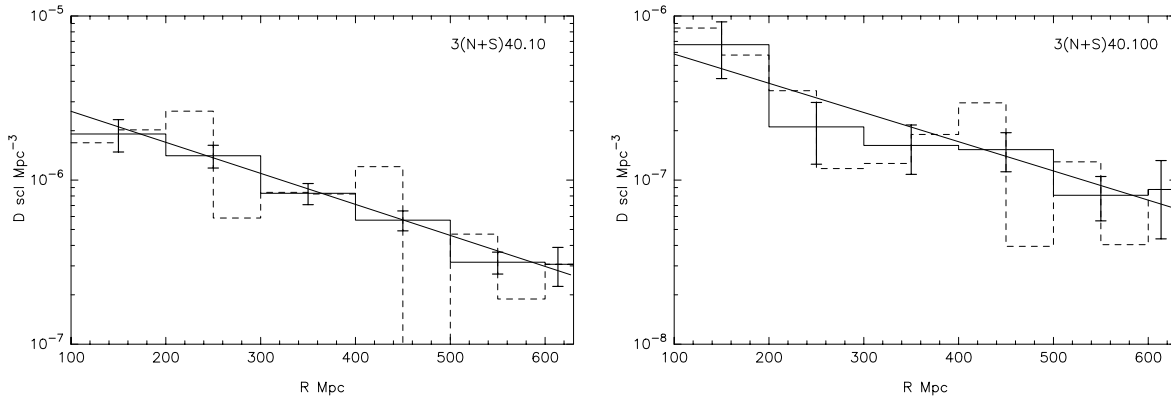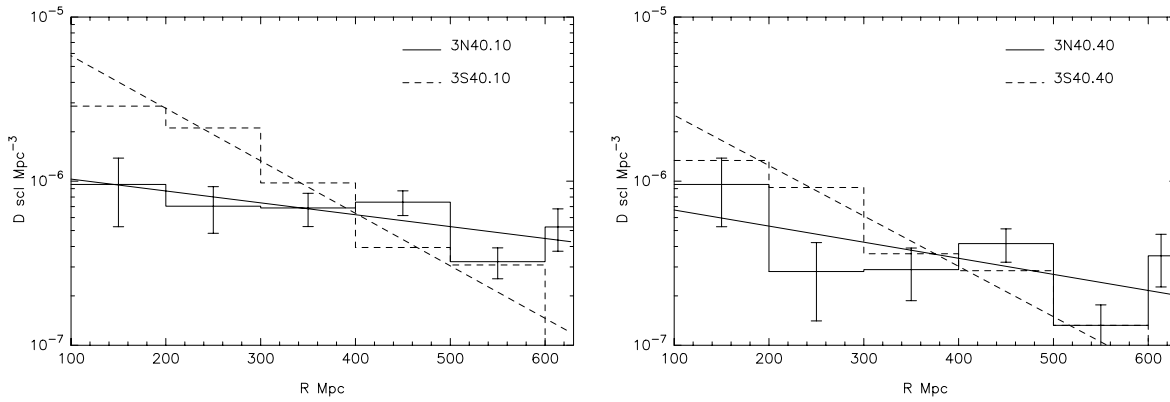
Fig. 10. Space density of superclusters from sample 3(N+S)40: left panel density enhancement 10, right panel 100

Fig. 11. Space density of superclusters from samples 3N40 and 3S40: left panel density enhancement 10, right panel 40

Table 6. Linear regressions $\log D = a + b\,R$

Sample	$-a$	Δa	$-b.10^3$	$\Delta b.10^3$	$-r$	s
3(N+S)40.10	5.392	0.045	1.89	0.10	0.99	0.040
3(N+S)40.20	5.452	0.070	2.07	0.16	0.99	0.063
3(N+S)40.40	5.72	0.15	1.82	0.34	0.94	0.13
3(N+S)40.100	6.05	0.16	1.78	0.36	0.93	0.14
3(N+S)40z.10	5.32	0.12	3.02	0.28	0.98	0.11
3N40.10	5.92	0.13	0.72	0.30	0.77	0.12
3S40.10	4.92	0.16	3.20	0.37	0.97	0.14
3N40.20	5.89	0.20	1.12	0.45	0.78	0.18
3S40.20	5.09	0.12	3.06	0.27	0.98	0.11
3N40.40	6.08	0.28	0.98	0.64	0.61	0.25
3S40.40	5.29	0.16	3.07	0.36	0.97	0.14
3N40z.10	5.692	0.096	1.91	0.22	0.97	0.086
3S40z.10	4.82	0.51	4.9	1.3	0.90	0.41
2(N+S)40.10	5.056	0.093	1.81	0.22	0.97	0.083
2N40.10	5.661	0.060	0.52	0.14	0.88	0.054
2S40.10	4.59	0.20	2.97	0.46	0.96	0.18
2N40.400	5.81	0.22	0.92	0.50	0.68	0.20
2S40.400	5.33	0.16	2.05	0.36	0.94	0.14

ter searching procedure, we could assume that many doublets are illusory superclusters. But this is not the case, since the regression for the sample 2(N+S)40.10 is almost parallel to the regression for the sample 3(N+S)40.10 (Table 6).

5. Voids among superclusters

Many attempts have been undertaken to define and to characterize voids in the distribution of galaxies and clusters, but there were not sufficient statistics for superclusters. The KK catalog gives an opportunity to study the voids among superclusters.

Let us consider the probability that a disk of area A randomly placed on the 2D distribution of superclusters contains no superclusters. According to White (1979), the 2D void probability function (VPF), namely $P(\Sigma\,A)$, where Σ is the 2D mean density, depends on the correlation functions of all orders. It is easy to show that for a Poisson distribution of points

$$P(\Sigma\,A) = \exp\left(-\Sigma\,A\right). \tag{8}$$

The VPF has been the most used statistic for void studies (e.g. Ostriker & Strassler 1989, Babul & Postman 1990, Maurogordato et al. 1992, Vogeley et al. 1994, Ghina et al. 1996).

We have applied the VPF to some supercluster samples (Fig. 12). Continuous lines refer to the theoretical VPF, while squares are the observed VPF with Poisson error. Each square is a result of 10000 simulations of the supercluster catalogs obtained by the bootstrap resampling technique. Of course, all randomly distributed disks intersecting the edge were rejected.

Clearly there are no significant voids in the 2D distribution of the superclusters. Having in mind that the superclusters are not points, one would expect even better agreement with a Poisson distribution.

Therefore, the 2D distribution of the voids among superclusters is Poissonian.

Voids in the 3D case, if any, should be named *supervoids*. The space distribution of the voids essentially depends on a decrease of the mean density D of superclusters with distance. The corresponding VDF is

$$P(DV_r) = \exp(-DV_r), \tag{9}$$

where V_r is a sphere of radius r which does not contain any supercluster, randomly placed among the real superclusters.

Therefore

$$P(DV_r) = \exp[\text{dex}(a + bR)V_r] = P(R, r), \tag{10}$$

where the coefficients are from Table 6. Note that the VDF depends on the distance and the radius of the empty spheres.

The observed VDF is derived again from random supercluster catalogs but without bootstrap resampling technique. Each random supercluster is simulated with distance according to linear regressions from Table 6 and random galactic coordinates.

But a comparison between observed and theoretical VPF is not so simple as the 2D case since there is an additional parameter, namely the radius r.
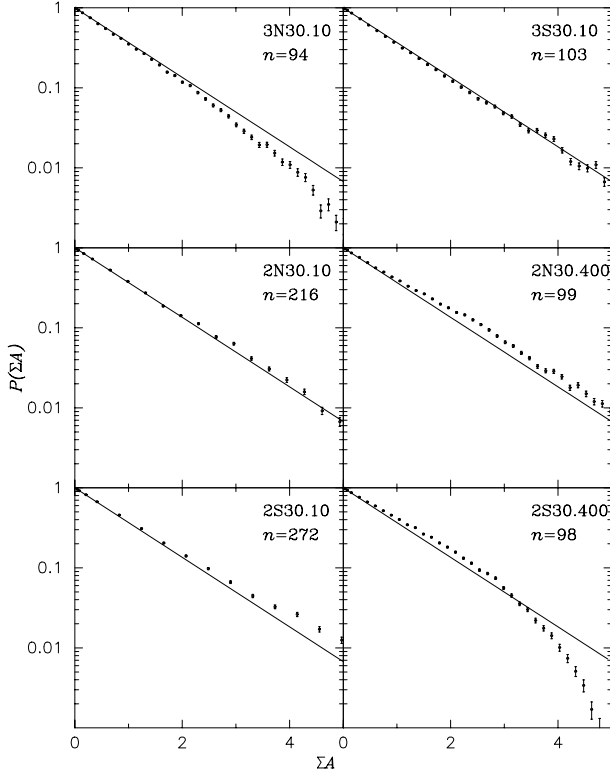
Fig. 12. Void probability functions (2D) for some samples. Continuous lines refer to $P(\Sigma A) = \exp(-\Sigma A)$. Each point of observed VPF is a result of 10 000 simulations. The uncertainties are Poisson errors

Fig. 13. Void probability functions (3D) for two samples. Curves are theoretical $P(R, r)$, while squares are observed VDFs. Radii of empty spheres are $r = 40, 60, 80$ and 100 Mpc.

Some results are presented in Fig. 13 for samples 3N40 and 3S40. The curves refer to theoretical, and squares to observed VPFs. Radii $r = 40, \ 60, \ 80$ and 100 Mpc are given. Each square is the result of 10000 random supercluster catalogs.

In general, the agreement between theory and observation is very good. Squares in the first bin ($100 \le R$ Mpc < 200) are biased estimates, since the volume where random supercluster centers are generated is smaller in order to avoid edge-on effects.

Fig. 13 shows that there is no definitive excess of observed over theoretical VPF. All samples of Table 1, having large size, say $n \gtrsim 60 \div 70$, lead to the same result. Hence supervoids among superclusters in real space do not exist with volume in the range $(1.1 \div 41.9) \cdot 10^5$ Mpc.

6. Correlation functions

Correlation functions are very powerful instruments to study the distribution of galaxies and clusters (Totsuji & Kihara 1969, Peebles 1973, 1980). It is established that the two-point space correlation functions of galaxies and clusters are power laws (with many modifications for dependence on the sample, luminosity, morphological type, richness etc.). But there is no agreement about the two-point space correlation function $\xi_{s-s}(r)$ for superclusters of galaxies.

The first determination of $\xi_{s-s}(r)$ was given by Kalinkov & Kuneva (1985). It is shown that $\xi_{s-s}(r) \approx 0$ for r h$^{-1} \lesssim 200$ Mpc. Bahcall & Burgett (1986) have used the catalog of super-

clusters of Bahcall & Soneira (1983) to estimate the correlation function. Assuming the same power index as for galaxies and clusters, Bahcall & Burgett conclude

$$\xi_{s-s}(r) = 1500 \ r^{-1.8} \approx (r/60)^{-1.8}. \qquad (11)$$

Moreover, based on the galaxy and cluster correlation functions

$$\xi_{g-g}(r) = 20 \ r^{-1.8} \text{ and } \xi_{c-c}(r) = 360 \ r^{-1.8}, \qquad (12)$$

they presume the existence of a dimensionless or universal correlation function (such a function is discussed by Szalay & Schramm 1985, also). The universal function is quoted in many papers – e.g. Bahcall & West (1992).

First of all, Fig. 1 in Bahcall & Burgett (1986) is not convincing, because of the scatter of the six points in the range 90–140 Mpc. But the scatter in their Fig. 2 is even larger.

Kalinkov & Kuneva (1986) used another catalog of superclusters with conclusions:

(i) the superclusters are almost uniformly distributed,
(ii) $\xi_{s-s}(r)$ has nothing to do with $\xi_{g-g}(r)$ and $\xi_{c-c}(r)$ and
(iii) the crosscorrelation function for rich-poor superclusters shows a weak anticorrelation.

Lebedev & Lebedeva (1988) have computed $\xi_{s-s}(r) = (r/90)^{-1.8}$ for the supercluster catalog of Batuski & Burns (1985a); this is a doubtful result because selections in the real catalog are not fully taken into account. Besides, the supercluster catalog is polluted, because of a crude estimation for redshift.

Now it is possible to compute $\xi_{s-s}(r)$ for more superclusters and for various density enhancements.

We use the standard estimate

$$\xi_{s-s}(r) = \frac{DD}{DR} \frac{2N}{N-1} - 1, \tag{13}$$

where DD is the number of supercluster pairs in the examined sample with space separation between $r - \Delta r/2$ and $r + \Delta r/2$, and DR is the number of pairs in a cross correlation between the observed supercluster catalog and a simulated one. The objects in the mock catalog are in an identical volume and are subject to the same selection effects presented in the observed sample. The sample size is N. So the mock catalog contains just the same number of objects as the real one. We use for the uncertainty of the correlation function

$$\Delta\xi = \frac{1+\xi}{\sqrt{DD}} = \sqrt{\frac{1+\xi}{DR}}. \tag{14}$$

Let us mention that the Hamilton (1993) estimator, namely

$$\xi_{s-s}(r) = 4\frac{DD\ RR}{DR^2} - 1, \tag{15}$$

leads to the same results when (13) is used.

Various simulated catalogs with different assumptions are generated.

(i) One attributes to each "random" point a triple of coordinates – b, l and distance R, which is taken from the real sample – it is a bootstrap resampling technique (bbb).

(ii) Cumulative distributions of b, l and R from the real sample are fitted with polynomials, which are used for generation of the simulation catalogs. The polynomials used are between 3rd and 14th order (ppp).

(iii) Cumulative distributions are fitted with straight lines only (111).

(iv) Mix procedures – (bbn), (bnn), (1nb)...

(v) Selection functions for b and R, uniformly distributions for l.

Obviously polynomials of higher order would produce catalogs very close to bootstrap resampling ones. But polynomials of first power, straight lines, operate as a function which smooths at the most possible degree. So the limiting cases, within which the real correlation function must be located, correspond to the bootstrap and polynomials of first power.

All calculated correlation functions are in the range defined by cases (bbb) and (111). However sometimes, when cumulative distributions are badly fitted with straight lines, the estimates according to (111) differ substantially from all other estimates.

In general, the first distance bin contains a biased estimate of the correlation function, since in the real samples there are no separations smaller than the diameters of the superclusters, while in the mock catalogs these separations could be smaller. In a more refined procedure for estimation of any correlation function, a cut-off parameter, or a softening distance, must be introduced.
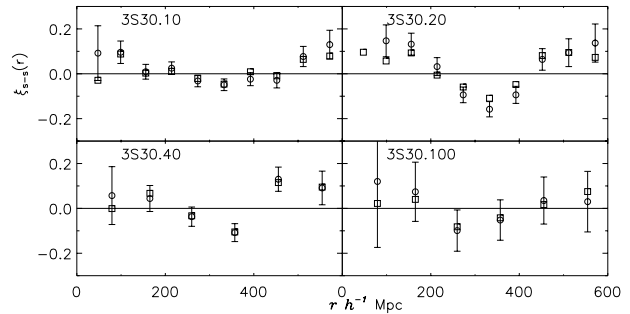
Each correlation function is determined for 1000 "random" catalogs and in the examined cases all (i) – (v) various estimates do not differ substantially.
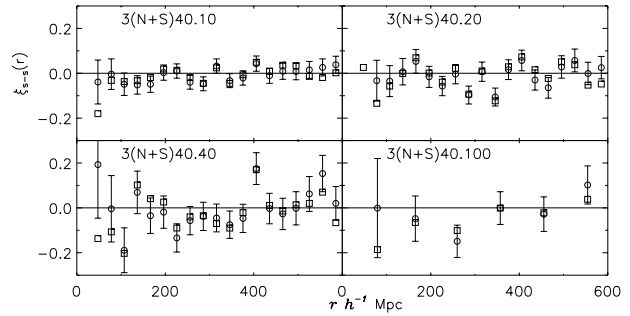
Fig. 14. Correlation functions for samples 3(N+S)40. Squares – bootstrap method (bbb), circles – polynomial fitting (111)
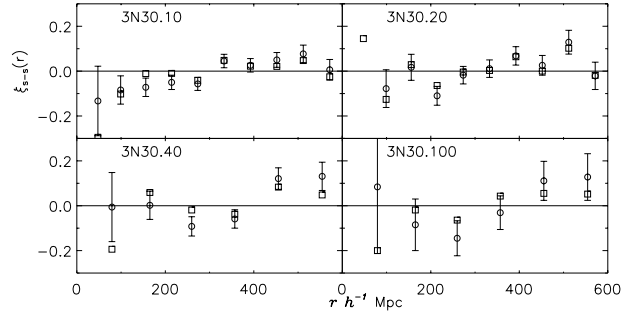
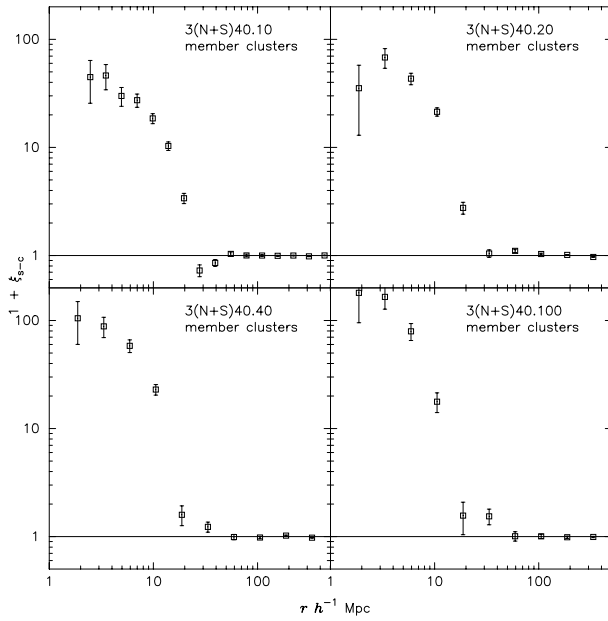**Fig. 15.** Correlation functions for samples 3N30

Fig. 16. Correlation functions for samples 3S30

Fig. 14 presents $\xi_{s-s}(r)$ for samples 3(N+S), and it is zero in the entire range of separations to 600 h^{-1} Mpc. One should note that, depending on bin, the first point of the smallest one is a biased estimate of the correlation function.

The same situation exists for samples 3N30 (Fig. 15). But for sample 3S30 (Fig. 16), there are indications for anticorrelation between 200 and 400 h^{-1} Mpc at all density enhancements. This might be due to uncertain redshift estimates.

The application of other estimators, including Landy & Szalay (1993), does not change the results (Kalinkov et al. 1997). Consequently the 2-point space correlation function of the superclusters is zero in the range $100 < R$ Mpc < 627.

We have attempted to estimate the correlation function as a function of the separation parallel and perpendicular to the line of sight, namely $\xi(r_p, \pi)$, e. g. Fisher et al. (1994). All attempts

Fig. 17. Crosscorrelation functions for superclusters and member clusters

Fig. 18. Crosscorrelation functions for superclusters and all clusters

failed $-\xi(r_p, \pi)$ is zero along as well as transverse to the line of sight.

This result that the correlation function is zero means there are no distortions in redshift space. Therefore, the correlation function in real space is zero too.
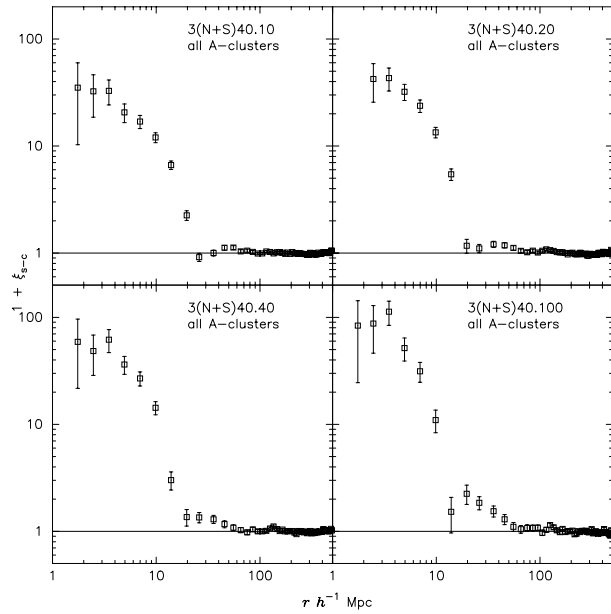
Up to now, we have been examining the autocorrelation function. Here some results on the crosscorrelation function will be given. All estimates are obtained with the bootstrap resampling technique.

Our calculation of the crosscorrelation function ξ_{s-c} for superclusters and clusters show no systematic difference between north and south caps. Therefore, only the crosscorrelation function for merged samples worth examining.

The crosscorrelation function for superclusters and member clusters is given in Fig. 17, while Fig. 18 presents the crosscorrelation function with all A- and ACO-clusters. In fact $1 + \xi_{s-c}$ is given. Of course only clusters located in the same volume defined for the superclusters are treated.

According to Fig. 17, the amplitude and the correlation radius of ξ_{s-c} increase when the density contrast increases. Fig. 18 establishes that "field" clusters of galaxies which do not belong to any supercluster are not correlated with the superclusters. Naturally, the corresponding amplitudes for member clusters are higher than for all clusters.

Crosscorrelation functions were determined for clusters and galaxies (Seldner & Peebles 1977; more details in Peebles 1980) and Stevenson et al. (1985). Lilje & Efstathiou (1988) proposed another model for the crosscorrelation function. However the supercluster-cluster crosscorrelation function cannot be fitted with the models applicable to the cluster-galaxy crosscorrelation function.

7. Reliability of the results

We use superclusters that have member clusters with estimated redshift. This could be regarded as a serious objection against our results. That is why some tests are presented in this section to verify the influence of the redshift estimates on our conclusions.

First we note that a naive assumption that estimated redshifts would "smear" any weak correlation (if any) is not correct. Suppose we estimate cluster redshift with one estimator only – the magnitude of the tenth rank galaxy. It is known that the distribution of m_{10} is clumpy, due to systematic effects (cf. Rowan-Robinson 1972). Then redshift estimates would be clumpy also, and preferred redshifts would appear. In a sense, the distances to clusters will be discrete and not continuous. Therefore the correlation would grow. This effect would be attenuated if there are several carefully selected estimators as in the our case.

We need to obtain the correlation function for samples containing only those superclusters having measured redshift for all cluster members. The sample sizes are not large and natural uncertainties would be larger. Secondly, if the KK catalog is not substantially different from other catalogs, we would expect the same correlation function for superclusters found according to quite different searching criteria. Finally a dependence of $\xi(r)$ on distance R could be tested when samples of near and distant superclusters are examined.

7.1. Correlation function for superclusters with measured redshift

We have created some samples of superclusters with measured redshift for all cluster members. The new samples are denoted with zz instead of z. The results for samples 3N30zz.10 (n = 40), 3S30zz.10 (n = 28) and 3(N+S)zz.10 for the bbb method are given in Fig. 19. Again 1000 random catalogs of superclus-
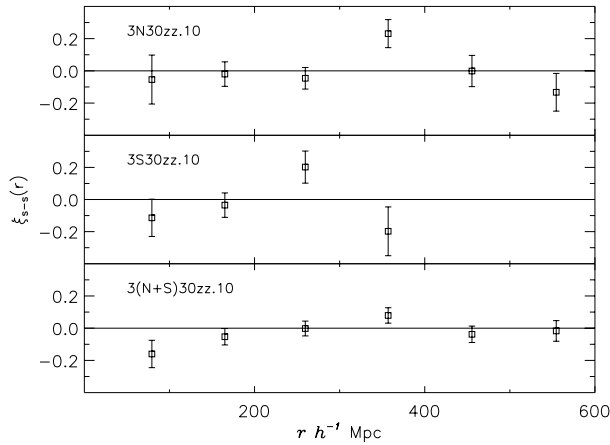
Fig. 19. Correlation function for superclusters with member clusters having measured redshift

Fig. 20. Correlation functions for superclusters from other catalogs

ters are used. Again, the correlation function is zero, which is very strong evidence that results presented in Figs. 14-16 are consistent. The consistency is manifested for the other samples and for different density enhancements.

Now let us look at a sample, denoted as 3N30zc which together with 3N30zz constitute the sample 3N30. The sample 3N30zc includes samples 3N30z and 3N30c – containing superclusters with cluster members without measured redshift. In the light of previous results, it is not surprising that $\xi(r) \approx 0$ for 3N30zc.10 as well as for 3S30zc.10.

7.2. Correlation function for other catalogs

The correlation functions for three other catalogs are presented in Fig. 20:

i) Zucca et al. (1993) – ZZSV, 69 superclusters for their $f \geq 2$ and $\nu \geq 2$,

ii) Einasto et al. (1994) – EETDA, 130 superclusters with $\nu \geq 2$ and

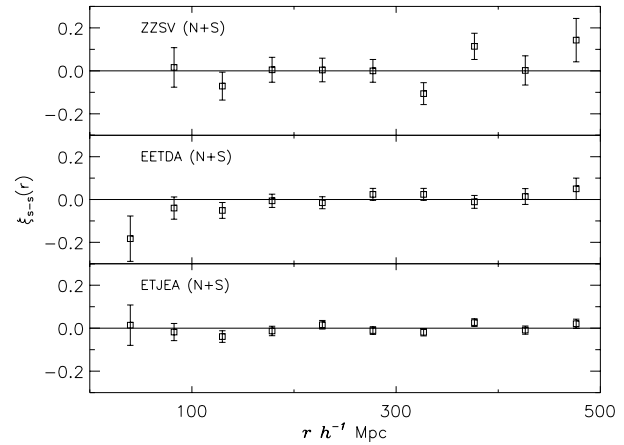**iii)** Einasto et al. (1997b) – ETJEA, 220 superclusters with $\nu \geq 2$.

Again the bbb method is used and 1000 simulated catalogs are generated for each case.

For all catalogs $\xi(r) \approx 0$. Therefore the zero correlation is an intrinsic property of all superclusters found, independent of the searching procedure.
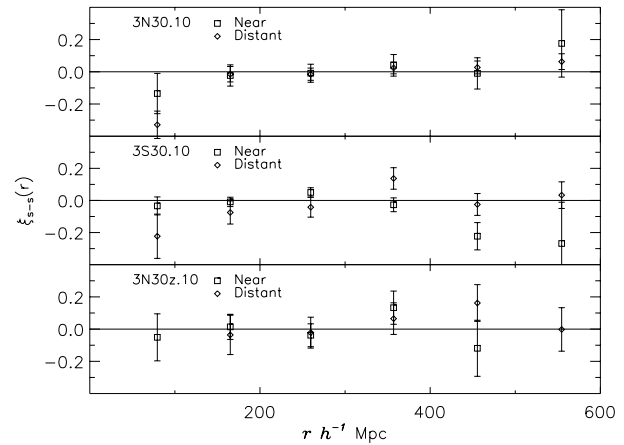
7.3. Correlation function for near and distant superclusters

Let us name *near* superclusters those having $100 \leq R$ Mpc < 400. Then *distant* superclusters have $400 \leq R$ Mpc < 627. Results for samples 3N30.10, 3S30.10 and 3N30z.10, containing respectively 44, 82 and 33 near, and 82, 49 and 31 distant superclusters are given in Fig. 21.

Obviously the incompleteness in the basic cluster catalog does not substantially affect the conclusions.

Fig. 21. Correlation function for near and distant superclusters

8. Discussion

The main result of this paper is that superclusters are uniformly distributed in space. If so, according to older terminology based on Abell and Zwicky discussions, clusters of galaxies of third order do not exist. (A galaxy is a cluster of zero order, a cluster of first, and a supercluster of second order.) Therefore the hierarchical clustering has an upper bound. A very crude estimate of the upper bound is 100–200 h^{-1} Mpc, resulting mainly from the diameter of the largest superclusters of galaxies. But if the Universe is structureless at separations larger than 100–200 h^{-1} Mpc, it means that we reach a homogeneous Universe.

This problem is not a new one (cf. Sect. 1). Our estimate is in coincidence with the transition scale to a homogeneous Universe of Einasto & Gramann (1993), as well as with the crossover to an isotropic and homogeneous Universe of Scaramella et al. (1991).

Our independent rough estimate of the upper bound of the hierarchical clustering is in good agreement with spectral estimates (Peacock & West 1993, Vogeley et al. 1992, Fisher et al. 1993). Let us mention that the upper bound may be regarded as the cutoff in the multifractal distribution (e.g. Coleman &

Pietronero 1992, Guzzo et al. 1992, Baryshev et al. 1994, Di Nella et al. 1996, Labini & Pietronero 1996).

A short discussion needs be given concerning the wavelet transform. The authors of some papers claim that the wavelet analysis is the only multiscale technique. It is not quite true, since here we have shown that a classic technique with Gaussian smoothing (and filtering) functions works at multiscales. This technique has an advantage, which enables us to see the fundamental magnitude – the surface (or space) density. Moreover, although not so simple, the technique gives an opportunity to study the 3D case. We add that in some cases it is better than the adaptive kernel smoothing (Silverman 1986, Beers et al. 1991, Merritt & Tremblay 1994, Huang & Sarazin 1996).

We did not find any voids among superclusters in the 2D nor in the 3D case, in contrast to Einasto et al. (1997b). Moreover, we did not find any regularity in the supercluster distribution reported by Einasto et al. (1997a).

The second important result here is the estimate of the two-point space correlation function. It is established that $\xi_{s-s}(r) \approx 0$ for a huge range – up to $\sim 600\ h^{-1}$ Mpc. Our result does not agree with those of Bahcall & Burgett (1986). However this poses another question, about the reality of the universal correlation function (UCF), e.g. (Bahcall & West 1992).

At the insistence of an anonymous referee, we have looked thoroughly at the disagreement of Bahcall & Burgett (1986) and our results on the correlation functions. We have repeated some of their calculations. BB estimates of ξ for bins 85-110, 110-135 and 135-160 Mpc are 0.8, 0.1 and ~ 0.1, respectively. If the uncertainty for these bins are 0.6, as is shown in their Fig. 1, it is worth to examine only $\xi(85 - 110)$. Our estimate for this range is higher $\xi \approx 1.2$ (for $n = 15$ superclusters having $0.02 \leq z \leq 0.08$; 10 000 random catalogs), but with an uncertainty of 1.8, which is defined in the manner of BB – a "typical 1σ statistical error-bar, obtained by comparison with 10 000 random catalogs" (p. L37). In fact, the Poisson error is 0.6, but it is the smallest one. Another uncertainty follows from the bootstrap resampling method (Ling et al. 1986), which seems to overestimate the error (Mo et al. 1992, Shepherd et al. 1997) leading to 1σ error of 1.9. We use as the most plausible one the uncertainty introduced by Efron & Tibshirani (1986) and successfully applied by Shepherd et al. (1997) and Kalinkov et al. (1997). This uncertainty leads to an error of 1.6. Moreover, the other estimates of the correlation function (Landy & Szalay 1993 and Hamilton 1993) definitely show no significant correlation in a wide range of separations $60 \leq r\ h^{-1}$ Mpc ≤ 200 for the BS superclusters.

We have to note that the first bin (85-110 h^{-1} Mpc) contains separations connected with superclusters BS12, BS6 and BS9. We do not think BS12 is a real supercluster. It is conglomeration of two famous superclusters – Bootes and Corona Borealis, and a poor supercluster (Scl 679 of KK). All of the existing catalogs include Bootes and Corona Borealis as different entries. No other catalogs contain BS6(A1035+A1187). While the Abell cluster A1187 is a member of a supercluster in EETDA and ETJEA, A1035 is not a part of any known supercluster. Maybe BS9 is a phantom too, despite it is found in

larger configurations in EETDA and ETJEA but linked together with A-clusters without measured redshift. If the corresponding separations of superclusters BS12, BS6 and BS9 are not taken into account then the estimate $\xi(r)$ = DD/RR - 1 drops to zero even within the Poisson error.

Likely considerations hold for the f = 40 sample of superclusters, giving the conclusion that the correlation function is zero among BS superclusters. (A minor note – there is a misprint of the right ascension of A1367+A1656 supercluster, BS10; it is 12^h20^m instead of 11^h20^m).

References

Abell G.O., 1958, ApJS 3, 211
Abell G.O., Corwin H.G., Olowin R.P., 1989, ApJS 70, 1
Babul A., Postman M., 1990, ApJ 359, 280
Bahcall N.A., Burgett W.S., 1986, ApJ 300, L35 (BB)
Bahcall N.A., Soneira R.M., 1982, ApJ 262, 419
Bahcall N.A., Soneira R.M., 1983, ApJ 270, 20
Bahcall N.A., Soneira R.M., 1984, ApJ 277, 27 (BS)
Bahcall N.A., West M.J., 1992, ApJ 392, 419
Bahcall N.A., Batuski D.J., Olowin R.P., 1988, ApJ 333, L13
Baryshov Y., Labini F.S., Montuori M., Pietronero L., 1994, Vistas Astron. 38, 419
Batuski D.J., Burns J.O., 1985a, AJ 90, 1413
Batuski D.J., Burns J.O., 1985b, AJ 299, 5
Batuski D.J., Bahcall N.A., Olowin R.P., Burns J.O., 1989, ApJ 341, 599
Beers T.C., Forman W., Huchra J.P., Jones C., Gebhardt K., 1991, AJ 102, 1581
Biviano A., Durret F., Gerbal D., et al., 1996, A&A 311, 95
Chamaraux P., Cayatte V., Balkowski C., Fontanelli P., 1990, A&A 229, 340
Coleman P.H., Pietronero L., 1992, Phys. Rep. 231, 311
Di Nella H., Montuori M., Paturel G., Pietronero L., Labini F.S., 1996, A&A 308, L33
Einasto J., Gramann M., 1993, ApJ 407, 443
Einasto M., Einasto J., Tago E., Dalton G.B., Andernach H., 1994, MNRAS 269, 301 (EETDA)
Einasto J., Einasto M., Gottlöber S. et al., 1997a, Nature, 385, 139
Einasto M., Tago E., Jaaniste J., Einasto J., Andernach H., 1997b, A&AS 123, 119 (ETJEA)
Efron B., Tibshirani R., 1986, Stat. Sci., 1, 54
Escalera E., Macgillivray H.T., 1995, A&A 298, 1
Escalera E., Macgillivray H.T., 1996, A&AS 118, 519
Escalera E., Mazure A., 1992, ApJ 388, 23
Escalera E., Slezak E., Mazure A., 1992, A&A 264, 379
Fisher K.B., Davis M., Strauss M.A., Yahil A., Huchra J.P., 1993, ApJ 402, 42
Fisher K.B., Davis M., Strauss M.A., Yahil A., Huchra J.P., 1994, MNRAS 266, 50
Gaupillaud P., Grossmann A., Morlet J., 1984, Geoexploration 23, 85
Ghigna S., Bonometto S.A., Retzlaff J., Goltlöber S., Murante G., 1996, ApJ 469, 40

Grebenev S.A., Forman W., Jones C., Murray S., 1995, ApJ 445, 607

Guzzo L., Iovino A., Chincarini G., Giovanelli R., Haynes M.P., 1992, ApJ 382, L5

Hamilton A.J.S., 1993, ApJ 417, 19

Holmberg E.B., 1974, A&A 35, 21

Huang Z., Sarazin C.L., 1996, ApJ 461, 622

Kalinkov M, 1973, C.r. Acad. Bulg. Sci. 26, 855

Kalinkov M., 1974. In: Barbanis B., Hadjidemetriou J.D. (eds.) Galaxies and Relativistic Astrophysics, Proc. First Europ. Astron. Meet., Athens, 1972, Springer-Verlag, vol. 3, 142

Kalinkov M., 1976, Mem. Soc. Astron. Italiana 45, 637

Kalinkov M., 1977. In: Müller E. (ed.) Highlights of Astronomy 4, Part 1, Reidel, Dordrecht, 279

Kalinkov M., Kuneva I., 1985, Astron. Tsirk. (Moscow) No. 1409, 1

Kalinkov M., Kuneva I., 1986, MNRAS 218, 49p

Kalinkov M., Kuneva I., 1995, A&AS 113, 451 (Paper I, KK)

Kalinkov M., Kuneva I., Tomov B., Vlahova K., Yanev K., 1976, C.r. Acad. Bulg. Sci. 29, 453

Kalinkov M., Dermendjiev V., Staikov B., Kuneva I., Tomov B., 1978, In: Longair M.S., Einasto J. (eds.) The Large Scale Structure of the Universe. Symp. IAU No. 79, Dordrecht-Boston, 276

Kalinkov M., Kuneva I., Börngen F., Kalloglyan A., 1987, Astrophysics 26, 15

Kalinkov M., Kuneva I., Valtchanov I., 1994. In: Crabtree D.R., Hanisch R.J., Barnes J. (eds.) Astronomical Data Analysis Software and Systems III. ASP Conf. Ser. Vol. 61, San Francisco, 263

Kalinkov M., Stavrev K., Kuneva I., 1983. In: Abell G.O., Chincarini G. (eds.) Early Evolution of the Universe and Its Present Structure, IAU Symp. 104, Reidel, Dordrecht, 185

Kalinkov M., Valtchanov I., Kuneva I., 1997 (submitted to ApJ)

Karachentsev I.D., Shcherbanovski A.L., 1978, AZh 55, 449

Labini F.S., Pietronero L., 1996, ApJ 469, 26

Landy S.D., Szalay A., 1993, ApJ, 412, 64

Lebedev V.S., Lebedeva I.A., 1988, Letters to AZh 14, 18

Lilje P.B., Efstathiou G., 1988, MNRAS 231, 635

Ling E.N., Frenk C.S., Barrow J.D., 1986, MNRAS 223, 21p

Maurogordato S., Schaeffer R., da Costa L.N., 1992, ApJ 390, 17

Merritt D., Tremblay B., 1994, AJ 108, 514

Mo H.J., Jing Y.P., Börner G., 1992, ApJ, 392, 452

Murray S.S., Forman W., Jones C., Giacconi R., 1978, ApJ 219, L89

Nichol R.C., Connolly A.J., 1996, MNRAS 279, 521

Olowin R.P., Chincarini G., Corwin H.G., 1987, Bull. AAS 19, No. 4

Ostriker J.P., Strassler M., 1989, ApJ 338, 579

Peacock J.A., 1991, MNRAS 253, 1p

Peacock J.A., Nicholson D., 1991, MNRAS 253, 307

Peacock J.A., West M.J., 1992, MNRAS 259, 494

Peebles P.J.E., 1973, ApJ 185, 413

Peebles P.J.E., 1980, The Large-Scale Structure of the Universe. Princeton Univ. Press

Postman M., Huchra J.P., Geller M.J., 1992, ApJ 384, 404

Postman M., Spergel D.N., Sutin B., Juszkiewicz R., 1989, ApJ 346, 588

Press W., Teukolskiy S., Vetterling W., Flannery B., 1992, Numerical Recipes in FORTRAN. Sec. edition. Cambridge Univ. Press, p. 281

Romani R. W. & Maoz D. 1992, ApJ 386, 36

Rood H.J., 1976, ApJ 207, 16

Rood H.J., 1979, ApJ 233, 431

Rowan-Robinson M., 1972, AJ 77, 543

Scaramella R., Vettolani G., Zamorani G., 1991a, ApJ 376, L1

Scaramella R., Zamorani G., Vettolani G., Chincarini G., 1991b, AJ 101, 342

Seldner M., Peebles P.J.E., 1977, ApJ 215, 703

Shane C.D., Wirtanen C.A., 1954, AJ 59, 285

Shane C.D., Wirtanen C., 1967, Publ. Lick Obs. 22, Part 1

Shepherd C.W., Carlberg R.G., Yee H.K.C., Ellingson E., 1997, ApJ 479, 82

Silverman B.W., 1986, Density Estimation for Statistics and Data Analysis, London, Chapman & Hall

Slezak E., Bijaoui A., Mars G., 1990, A&A 227, 301

Slezak E., de Lapparent V., Bijaoui A., 1993, ApJ 409, 517

Slezak E., Durret F., Gerbal P., 1994, AJ 108, 1990

Smoot G.F., et al., 1992, ApJ 396, L1

Stark A.A., Gammie C.F., Wilson R.W., et al., 1992, ApJS 79, 77

Stevenson P.R.F., Shanks T., Fong R., MacGillivray H.T., 1985, MNRAS 213, 953

Szalay A.S., Schramm D.N., 1985, Nat 314, 718

Thuan T.X., 1980. In: Balain R., Audouze J., Schramm D.N. (eds.) Physical Cosmology. Amsterdam, North Holland, 277

Totsuji H., Kihara T., 1969, PASJ 21, 221

Tully R.B., 1987, ApJ 323, 1

Vogeley M.S., 1995, preprint

Vogeley M.S., Park C., Geller M.J., Huchra J.P., 1992, ApJ 391, L5

Vogeley M.S., Geller M.J., Park C., Huchra J.D., 1994, AJ 108, 745

West M.J., 1989, ApJ 347, 610

White S.D.M., 1979, MNRAS 186, 145

Zucca E., Zamorani G., Scaramella R., Vettolani G., 1993, ApJ 407, 470 (ZZSV)